RECONSTRUCTIVE ULTRASOUND ELASTICITY IMAGING FOR RENAL PATHOLOGY DETECTION

S.Y. Emelianov,[13] M.A. Lubinski,[1] A.R. Skovoroda,[3] R.Q. Erkamp,[1]
S.F. Leavey,[2] R.C. Wiggins,[2] and M. O'Donnell[1]

[1] Biomedical Engineering and Electrical Engineering & Computer Science Departments, and
[2] Division of Nephrology, Department of Internal Medicine, University of Michigan, Ann Arbor, MI 48109, and
[3] Institute of Mathematical Problems of Biology, Russian Academy of Sciences, Pushchino, Russia, 142292

Abstract – The real-time capability of ultrasound is it's major advantage for reconstructive elasticity imaging. In addition to providing important immediate feedback during patient examination, real-time data capture provides an excellent means for retrospective data processing. With retrospective processing, normal axial strain images can be optimized for highest SNR, the accuracy of lateral displacement estimates can be improved, and finally, non-linear elastic properties of tissue can be evaluated resulting in contrast enhancement of elasticity imaging. Retrospective processing requires no new data capture and adds new important features to reconstructive ultrasound elasticity imaging.

INTRODUCTION

Assessing the degree of renal scarring, and distinguishing interstitial fibrosis from acutely inflamed or normal kidney provides critical information required to guide therapy in normal and transplanted kidneys. Renal biopsy can determine the degree of interstitial fibrosis and acute inflammation in a transplant kidney, but frequent biopsies are not feasible for screening because of the associated risks and cost. Since kidney elasticity is expected to change dramatically with scar formation, and to lesser degree with acute inflammation or edema, elasticity imaging can possibly be used to diagnose and monitor kidney transplant rejection [1], [2].

The major advantage of ultrasound for elasticity imaging is it's inherent real-time capabilities. In addition to immediate feedback about patient position and comfort during the examination, etc., real-time data acquisition provides an excellent foundation for retrospective processing of data captured during slow, continuously applied surface deformations [1].

The goal of retrospective processing is threefold. First, estimates of internal strain can be greatly optimized for the highest possible strain SNR throughout the entire image plane using **adaptive speckle tracking** [1], [3]. Second, the diffraction limited accuracy of lateral displacement estimates can be improved using **incompressibility processing** [4]. Finally, for large surface deformations, **adaptive elasticity imaging** is required to handle the non-linear elastic properties of tissue and to enhance elasticity image contrast.

In this paper, two approaches to retrospective data processing were investigated: adaptive speckle tracking for strain imaging [1], [3], and adaptive elasticity imaging for large deformations.

RETROSPECTIVE DATA PROCESSING

In reconstructive elasticity imaging, data are captured periodically during continuously applied surface deformation. Therefore, the average frame-to-frame surface deformation is approximately uniform. The internal strain distribution, however, is not generally uniform throughout the imaging plane even for a simple homogeneous object. Since both displacement and strain errors depend on the magnitude of the internal strain, only a fraction of the image will exhibit optimal signal to noise ratio (SNR).

To overcome this problem, adaptive speckle tracking for strain imaging was proposed [1], [3]. In adaptive speckle tracking, strains are estimated using a decimated number of frames, where the specific frame decimation ratio is adapted on a point for point basis to optimize strain SNR throughout the image. The frame decimation ratio is determined by the strain intensity at a particular position. In regions where internal strain is high, every frame must be used. However, for low internal strain regions, a high decimation ratio should be used. Finally, displacement and strain estimates for multiple frame decimation ratios are combined to produce an optimized strain image. Since strain SNR is proportional to the magnitude of the surface displacement normalized to the correlation coefficient, the slope of correlation coefficient as a function of surface displacement is used to guide adaptive speckle tracking. Although this procedure is complex, no new data are needed.

Most soft tissues exhibit non-linear elastic properties. This is especially true if large surface deformations are applied to achieve high SNR strain images. In addition, these non-linear elasticity-strain dependencies are not known *a priori*. Adaptive elasticity imaging, however, can estimate the non-linear elastic properties of tissue through retrospective processing of real-time data captured over the entire deformation range. The basic principle is that elasticity reconstruction can be performed for small subsets of data spanning the entire deformation range. Within each subset, the elasticity (Young's modulus) can be well approximated as a constant permitting reconstruction based on a linear elastic model. However, since each subset is associated with a different overall internal strain, the non-linear elastic properties of tissue can be evaluated. Again, retrospective processing for adaptive elasticity imaging requires no new data.

To illustrate the applicability and potential of adaptive speckle tracking and adaptive elasticity imaging for renal

0-7803-4153-8/97/$10.00

pathology diagnosis, experiments were performed using an *ex-vivo* kidney model.

MATERIALS AND METHODS

Experiments were performed on fresh canine kidney embedded in an otherwise homogeneous gel. The 140-mm by 100-mm by 80-mm phantom was placed in the deformation system so that the transverse plane of kidney could be imaged. Therefore, the longest axis of the rectangular phantom was perpendicular to the axis of a 128 channel, 1-D transducer array operating at 5 MHz. The transducer was mounted with a rigid pad to increase the area over which surface deformations could be applied. Large (16 percent average strain) deformations of the phantoms were produced by 12.8 mm surface displacement of a rigid pad with attached transducer. These deformations were applied continuously using a manually controlled 1-D motion axis.

During surface deformation over the 4 second interval, more than 120 consecutive frames of digital radio frequency (RF) data output by the beamformer of an ATL "Ultramark-9" HDI clinical ultrasound scanner were nondestructively captured in real-time. Frame-to-frame motion was estimated using a two-dimensional correlation-based phase-sensitive speckle tracking technique which combines the ability of correlation-based algorithms to track large displacements with the precision of phase sensitive techniques. The 2-D displacement was estimated from the position of the maximum correlation coefficient, where the axial displacement estimate was refined by determining the position of the zero crossing of the analytic signal correlation. Displacement error was further reduced by filtering spatially adjacent correlation functions prior to displacement estimation. Four image sets corresponding to different frame decimation ratios (1, 2, 4, 8) were used in adaptive speckle tracking. Finally, estimates of displacement and strain for different decimation ratios were combined to create composite images with optimal strain SNR.

For adaptive elasticity imaging, deformation data were separated into six adjacent non-overlapping subsets covering the entire deformation range. Within each subset, the average strain is approximately 2 percent permitting linear elasticity reconstruction. Under a plane strain state (applicable in the current experimental setup and achievable in clinical practice) elasticity reconstruction requires accurate measurements of both axial and lateral components of the displacement vector, or similarly, normal axial and shear components of the strain tensor [5]. For each deformation subset as well as for the entire deformation experiment, the elastic modulus was linearly reconstructed based on measured displacements and strains using adaptive speckle tracking [1], [3]. In addition, the diffraction limited accuracy of lateral displacements was improved using incompressibility processing [4]. The Young's modulus was computed within a region of interest (ROI) containing the kidney approximately at the center and surrounded by gelatin. Along the boundary of this 32.5-mm by 54-mm ROI, the Young's modulus was set to a constant providing the necessary boundary conditions for relative elasticity reconstruction inside the ROI. The linear elasticity equations describing a plane strain deformation of the phantom were discretized with a 2 mm sampling grid. The linear equations resulting from discretization of the elasticity equations were solved by iteration [5].

The first deformation experiment was performed on an unaltered canine kidney. Once these data were captured and stored for off-line retrospective processing, a needle was inserted into the phantom, and one ml of 15% glutyraldehyde solution was injected into the kidney parenchyma to create a localized "lesion". Deformation measurements were repeated (approximately every 40 minutes for up to 3½ hours), imaging precisely the same kidney cross-section. Finally, at the conclusion of the experiment, the phantom was cut along the imaging plane and photographed.

RESULTS AND DISCUSSION

A typical B-scan of the phantom is shown in Fig. 1. A 38-mm by 80-mm area of the phantom in the initial (i.e., prior to deformation) position is presented. The transverse view of the kidney can be clearly identified. Prior to the experiment, the phantom was slightly pre-deformed to insure secure contact between the transducer plate and the surface of the phantom. The arrow in this figure indicates the path and final position of the needle during glutyraldehyde injection.

Adaptive speckle tracking is illustrated in Figs. 2 and 3. In figure 2, the normal axial strains computed with different frame decimation ratios (1, 2, 4 and 8, respectively) are displayed over the same 0 to 30 percent strain range, where full white represents a normal axial strain of 30 percent and larger, and full black represent no strain. In all images, the region of highest strain magnitude is located in the interior part of the kidney. The strain magnitude in the outer part of the kidney is small and even lower than that in the surrounding phantom material. The noise in high strain regions is much smaller in Figs. 2a and 2b compared to Figs. 2c and 2d, mostly due to correlation peak hoping. In contrast, strain SNR in low strain regions is better in Figs. 2b-d compared to Fig. 2a. Note that all images in Fig. 2 are computed with the same spatial resolution.

The results presented in Fig. 2 suggest that the frame decimation ratio should be adapted for each image point to optimize strain SNR throughout the imaging plane. On a point by point basis, the best decimation ratio is selected using a correlation coefficient based weighting scheme. Resulting combined strain images are presented for unaltered kidney in Fig. 3a and for kidney 3½ hours after glutyraldehyde injection in Fig. 3b. High strain SNR is evident throughout the entire image in both Figs. 3a and 3b.

Changes in the kidney before and after injection are noticeable in the strain images of Fig. 3. Most evident is the region of glutyraldehyde injection where the strain magnitude is significantly reduced signaling a Young's elastic modulus increase. Overall, the entire kidney after the injection exhibits lower strain magnitude. Since the applied surface deformations are the same in both experiments, the overall increase of kidney elasticity after injection caused higher strain magnitude above the kidney (i.e., near the transducer surface).

Following adaptive speckle tracking for strain imaging, and estimating the lateral displacement using incompressibility processing, Young's modulus images were reconstructed. The images in Figs. 4a and 4c are 38-mm by

Figure 1

Figure 2a

Figure 2b

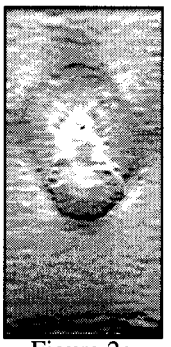

Figure 2c

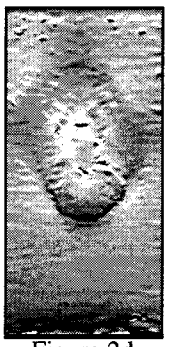

Figure 2d

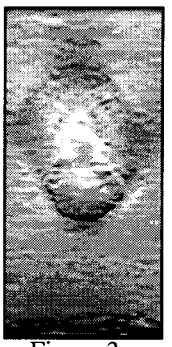

Figure 3a

Figure 3b

Figure 4a

Figure 4b

Figure 4c

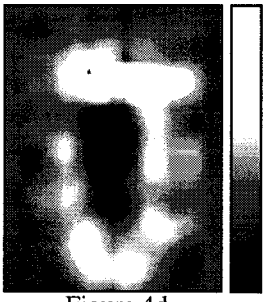

Figure 4d

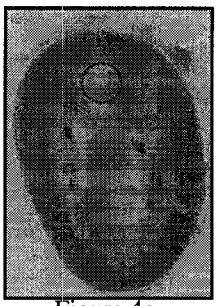

Figure 4e

Figure 5a

Figure 5b

Figure 5c

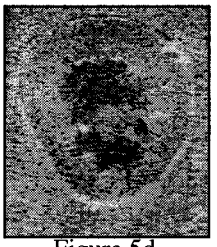

Figure 5d

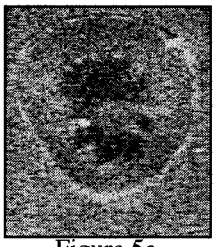

Figure 5e

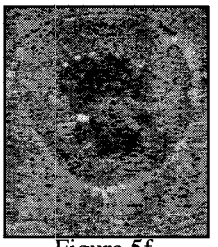

Figure 5f

Figure 6a

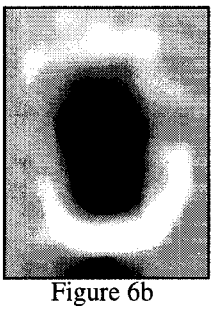

Figure 6b

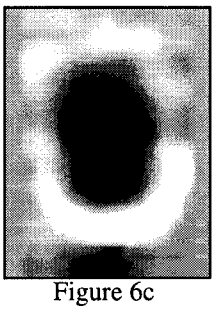

Figure 6c

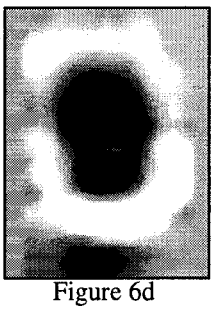

Figure 6d

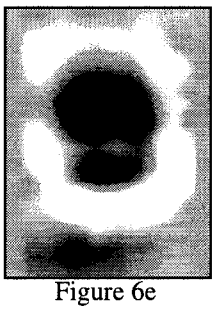

Figure 6e

Figure 6f

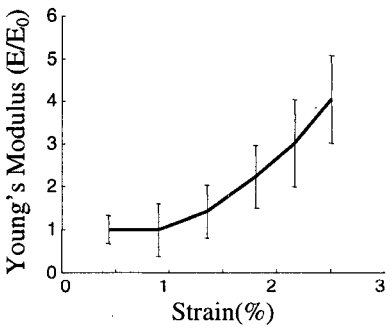

Figure 7a

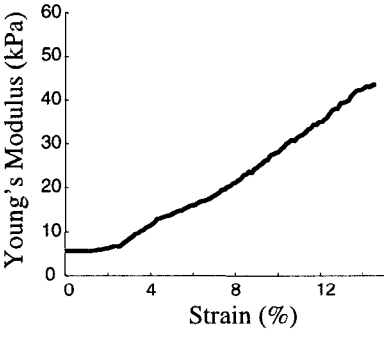

Figure 7b

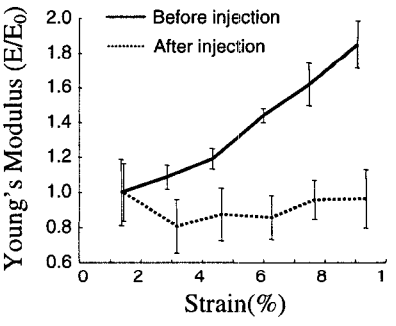

Figure 7c

43.5-mm B-scan regions containing the kidney before and after injection, respectively. In these images, there are no differences that can be *a priori* related to glutyraldehyde injection. The corresponding elasticity images in Figs. 4b and 4c, respectively, are 32.5-mm by 43-mm regions, where a logarithmic color map was used to display the relative Young's modulus over a 0.36 to 33 range. The color map is illustrated in the bar next to Fig. 4d. Clearly, the interior part of the kidney before injection appears to be softer compared to outer kidney regions. After injection, a localized "lesion" was created within the kidney as well as an overall kidney elasticity increase. The overall elasticity increase is also evident in Fig. 4d and is more likely related to glutyraldehyde diffusion over the duration of the experiment. A photograph of the kidney cross-section after the experiment clearly indicating the lesion is shown in Fig. 4e. In addition, manual palpation of the kidney cross-section qualitatively confirmed the elasticity distribution depicted in Fig. 4d.

The images presented in Figs. 4b and 4d demonstrate that elasticity imaging can detect changes in tissue state not evident from conventional ultrasound. Even these reconstructions are in slight error because a linear elastic model was used for large deformations. The elasticity reconstruction, however, need not be limited to a linear model and can be formulated to account for non-linear dependencies of displacement-strain and strain-stress relations.

The non-linear behavior of tissue elasticity can be estimated using adaptive elasticity imaging. The results of this approach are shown in Figs. 5 and 6 for the kidney before injection. Here, B-scan and elasticity images are presented for six adjacent subsets of the total deformation. All B-scans in Fig. 5 are 43-mm by 38-mm regions, and all elasticity (relative Young's modulus) images in Fig. 6 are 43-mm by 32.5-mm regions displayed over a 0.082 to 5.76 range. Also, all elasticity images in Fig. 6 are presented over the same geometry as the corresponding B-scan images in Fig. 5. For the first images in Fig. 5, the elasticity distribution is similar to the one in Fig. 4b, but displayed over a different range. However, as the total deformation increases, the cortex and medulla are more and more contrasted in the elasticity images. Also, the softer internal part of the kidney distinctly separates into two upper and lower regions. This closely resembles the structural features seen on the B-scans. Therefore, contrast enhancement is possible with adaptive elasticity imaging.

Quantitative analysis of adaptive elasticity imaging is given in Fig. 7. In figure 7a, the normalized relative Young's modulus is plotted as a function of total strain magnitude. Estimates were obtained from a 10-mm by 10-mm region positioned in the middle part of the kidney. In this figure and Fig. 7c, error bars indicate standard deviation values within the region. Clearly, non-linear elastic behavior of tissue (strain hardening) is evident. The results in Fig. 7a should be qualitatively compared with the results of direct mechanical measurements of the Young's modulus performed on a cylindrical 10-mm high by 7-mm radius sample from a similar canine kidney [6]. Note the overall similarity between Figs. 7a and 7b.

Adaptive elasticity imaging was also performed using deformation data from the kidney after injection. In figure 7c, strain dependencies of Young's moduli before and after injection are contrasted. Young's modulus estimates were obtained from the 10-mm by 10-mm region positioned in the lower portion of the kidney. Clearly, kidney parenchyma is highly non-linear before glutyraldehyde injection, and less after injection. These results strongly suggest that elastic non-linearity can be representative of tissue state.

In conclusion, the results of this study suggests strongly that elasticity imaging has the potential to become an important diagnostic tool of sufficient sensitivity and specificity for clinical practice and, in particular, can provide a safe means of non-invasive monitoring and diagnosis of early states of kidney transplant rejection [1], [2], [7].

ACKNOWLEDGEMENTS

Support from the National Institutes of Health under Grant DK 47324 is gratefully acknowledged. Many thanks to ATL for the "Ultramark-9" HDI imaging system.

REFERENCES

[1] M. O'Donnell, S.Y. Emelianov, A.R. Skovoroda, M.A. Lubinski, W.F. Weitzel, and R.C. Wiggins, "Quantitative elasticity imaging," in Proceedings of the IEEE Ultrasonics Symposium, 1993, pp. 893-903.

[2] S.Y. Emelianov, M.A. Lubinski, W.F. Weitzel, R.C. Wiggins, A.R. Skovoroda, and M. O'Donnell, "Elasticity imaging for early detection of renal pathologies," Ultrasound in Medicine and Biology, 21(7), pp. 871-883, 1995.

[3] M.A. Lubinski, S.Y. Emelianov, and M. O'Donnell, "Adaptive strain estimation using retrospective processing," IEEE Transactions on Ultrasonics, Ferroelectrics, and Frequency Control, in preparation, 1997.

[4] M.A. Lubinski, S.Y. Emelianov, K.R. Raghavan, A.E. Yagle, A.R. Skovoroda, and M. O'Donnell, "Lateral displacement estimation using tissue incompressibility," IEEE Transactions on Ultrasonics, Ferroelectrics, and Frequency Control, 43, pp. 234-246, 1995.

[5] A.R. Skovoroda, S.Y. Emelianov, and M. O'Donnell, "Reconstruction of tissue elasticity based on ultrasound displacement and strain images," IEEE Transactions on Ultrasonics, Ferroelectrics, and Frequency Control, 42, pp. 747-765, 1995.

[6] R. Erkamp, P. Wiggins, A. Skovoroda, S. Emelianov, and M. O'Donnell, "Gold standard system to measure the elasticity of small tissue samples," Ultrasonic Imaging, submitted for publication, 1997.

[7] S.Y. Emelianov, M.A. Lubinski, A.R. Skovoroda, R.Q. Erkamp, S.F. Leavey, R.C. Wiggins, and M. O'Donnell, "Reconstructive ultrasound elasticity imaging for renal transplant diagnosis: kidney ex-vivo results," Ultrasonic Imaging, submitted for publication, 1997.